CHAPTER 5

Photo-Fenton interfacial phenomena on graphene oxide: computational and experimental investigations

5.1. Introduction

Graphene oxides (GO) have been reported to be excellent adsorbents for many toxic dyes [Molla et al. (2019), Ramesha et al. (2011), Yan et al. (2014)], heavy metals [Bian et al. (2015), Li et al. (2015), Reynosa-Martínez et al. (2020)], organic pollutants [Phatthanakittiphong & Seo (2016), Thakur & Kandasubramanian (2019)], and antibiotics [Ai et al. (2019), Çalışkan Salihi et al. (2020)] from wastewater. The adsorption capacity of GO increases with its degree of oxidation [Bustos-Ramírez et al. (2015), Jiang et. al (2013), Thangavel & Venugopal (2014)]. Furthermore, a more oxidized GO has a wider bandgap than the less oxidized ones [Thangavel & Venugopal (2014)]. Also, the oxygen functionalities on the graphene sheet's surface make it compatible with polar solvents [Konios et al. (2014)] as well as hydrophilic [Thangavel & Venugopal (2014)]. These materials are thereby also suitable for catalytic and photocatalytic applications in an aqueous medium. Thus, Yeh et al. (2011) reported that the GO prepared in their lab had a visible range bandgap suitable for photocatalytic applications. Krishnamoorthy et al. (2011) analyzed the photocatalytic reduction of resazurin into resorufin on GO nanostructures. In a nutshell, the properties of each GO material produced in the lab could be different because of varying oxidation levels in them. The rich oxygen functionalities and good dispersibility of GO's in water are responsible for [Bustos-Ramírez et al. (2015), Jiang et al. (2013), Konios et al. (2014), Lee et al. (2016)] their adsorption, catalytic, and photocatalytic properties.

Jain et al. (2020), Nguyen et al. (2017), and Zhao et al. (2017) demonstrated that GO is an effective metal-free catalyst for advanced oxidation processes using H_2O_2. In such reactions (also called heterogeneous Fenton-like reactions), hydroxyl radicals ($^{\bullet}OH$) are formed by the catalytic activation of H_2O_2 molecules on the surface of solid catalysts. $^{\bullet}OH$ are potent but non-selective oxidants that oxidize and degrade organic pollutants

from wastewater [Deng & Zhao (2015), He et al. (2016)]. The conversion of H_2O_2 to water and oxygen at the end of a Fenton reaction makes it a green environmental remediation technique. GO materials with finite bandgaps can also act as photocatalysts for photo-Fenton oxidation of organic pollutants [Espinosa et al. (2016)].

Most experimental studies using GO as the heterogeneous Fenton or photo-Fenton catalyst do not give enough attention to the mechanism involved. The latter is critical for determining the design requirements for an efficient catalyst specific to a reaction. The mechanistic issues involved belong to two broad categories. The first type addresses the efficacy of the Fenton catalyst to activate the HO-OH bond for hydroxyl radicals. The other question relates to the adsorption/interaction of H_2O_2 and the target pollutant molecules with the catalyst surface in an aqueous medium. The reductive cleavage of H_2O_2 requires its effective interaction with nucleophilic sites on the catalyst for optimum $^{\bullet}OH$ generation in the aqueous solution of the organic pollutant. Chapter 4 of this thesis concluded that H_2O_2 and the target organic pollutant molecules should be nearby because the generated $^{\bullet}OH$ radical has a short lifetime. Two types of information are needed about the oxygen functionalities on a GO. First, to find the oxygen functionalities on GO that are nucleophilic. The second requirement is that H_2O_2 molecules should effectively adsorb or interact with these nucleophilic sites for optimum $^{\bullet}OH$ generation.

Similarly, for photo-Fenton reactions, the nucleophilic part of the photo-excited photocatalyst must actively interact with H_2O_2 molecules. The relative location and interaction of the organic pollutant molecules with respective oxygen functionalities are also critical because of the short lifetimes of $^{\bullet}OH$. This body of information is required to tailor GO nanostructures more suited for the targeted photo-Fenton catalyst action. Note that there is little or no research in the literature from this perspective. While Cortés-Arriagada et al. (2013) and Tang et al. (2018) reported pollutant molecules' interactions

with graphene and graphene oxide model sheets by quantum mechanics, no literature is available on the competition between reactants for specific sites on the GO surface in an aqueous medium. The nucleophilic sites are the GO oxygen functional groups with the highest occupied molecular orbital (HOMO) located on them. Suitable density functional theory (DFT) calculations can identify the HOMO positions on a catalyst [Verma et al. (2021), Verma et al. (2020)]. As mentioned in the earlier chapters, MD simulations have been used to elucidate the adsorbate-adsorbent interactions in a competitive aqueous reaction medium scenario. This information, combined with a suitable experimental investigation, can clarify the interfacial phenomena during a Fenton reaction over the catalyst surface, as discussed in chapter 4.

The present chapter investigates the Fenton (in the dark) and visible light photo-Fenton catalytic activities of two GO materials with different degrees of oxygen functionalities for orange-G (OG) dye degradation from the perspective mentioned above. OG is a water-soluble and acidic azo dye having extensive uses in textile applications. Improperly treated industrial effluents containing OG flow into natural water sources and pollute the environment [Sun et al. (2008), Tarkwa et al. (2019)]. The two GO's were synthesized by a modified Hummer's method but with different oxidation protocols. The prepared materials were characterized and used as catalysts and photocatalysts for OG degradation.

DFT calculations were performed on model GO structures with varying oxygen functionalities. An appropriate gap between the HOMO and the lowest unoccupied molecular orbital (LUMO) of the model structures led to the GO model being susceptible to visible light activation. Time-dependent density functional theory (TD-DFT) calculations were also carried out on this GO model (with a visible light HOMO-LUMO gap). Frontier molecular orbital theory images were used to locate the GO model's

nucleophilic and electrophilic functionalities. Then large-scale classical MD simulations in an aqueous medium were used to know how different reactants interact with particular oxygen functionalities on the GO structure. Finally, the experimental and computational results are combined to shed light on some critical aspects of heterogeneous Fenton and photo-Fenton mechanisms operating on a typical GO structure.

5.2 Experimental Methodology

5.2.1 Synthesis of G1 and G2 photocatalysts

Graphene oxide was synthesized according to the modified Hummer's method [Hummers & Offeman (1958), Hayes et al. (2015)]. Initially, 2.5g of graphite powder (Sigma Aldrich) and 2g of $NaNO_3$ (Merck) were mixed with 70 ml concentrated H_2SO_4 in a beaker kept in an ice bath. Next, potassium permanganate ($KMnO_4$: 10g) was added slowly under constant stirring. After completion of the mixing, the reaction mixture was removed from the ice bath and heated at 50°C for 6 hours. This step was followed by overnight cooling until the mixture became dark brown colored. The whole mixture was cooled and divided equally into two beakers. Then, added different amounts of $KMnO_4$ in these two beakers to prepare two types of GO (G1: 5g and G2: 4g of $KMnO_4$) with different oxidation levels. Subsequently, both G1 and G2 samples were heated at 35°C for another 12 hours. The solutions in the beakers were cooled to room temperature with 3ml of H_2O_2 (30wt.% H_2O_2, Merck). The mixture was allowed to stand for three days (until the appearance of a yellow-colored suspension). Then the mixture was centrifuged (at 6000rpm for 10 minutes), and the residue obtained was washed alternatively in 3wt.% H_2SO_4 and 0.5wt.% H_2O_2, repeatedly. These GO mixtures were then washed with distilled water until the pH of the washing was ~3. Both mixtures were then subjected to 5 hour ultrasonication for proper exfoliation. The sonicated suspensions were centrifuged at 9000 revolutions per minute, and the separated products were kept in a vacuum oven

overnight for drying. As mentioned earlier, G1 and G2 represent the two samples in the rest of this chapter.

5.2.2 Catalytic photo-Fenton experiment

The photo-Fenton catalytic activities of G1 and G2 samples were evaluated for the degradation of an OG (Merck) solution. A volume of 400µL of OG (132.6µM stock OG solution) was mixed with 2ml distilled water in a quartz cuvette (of 1cm path length). This solution's pH was adjusted to ~3.0 by adding 5µL of 0.1M HCl (Hydrochloric acid). Next, 100µL of catalyst (2mg in 4mL distilled water) suspension was added to the reaction mixture. The total solution was set aside for two hours to attain adsorption-desorption equilibrium under dark conditions and constant stirring. A magnetic stirrer was used for the mild stirring of the dispersion during the photocatalytic experiment. Such gentle stirring does not affect GO structure. Then, 6µL of H_2O_2 (30% H_2O_2: Merck) solution was added to this solution. The final reaction mixture was put under a cool white LED visible light source. The UV-visible spectrum of the reaction mixture was measured at regular intervals of time. The above procedure was repeated for evaluating the photo-Fenton activity of the G2 catalyst.

5.3 Computational Methodology

5.3.1 DFT details

Three GO models were constructed on the GaussView 6 graphical user interface. These structures have a varying number of functional groups (hydroxyl and epoxy groups). The empirical formulae of three model structures are $C_{54}H_{17}(O)_1(OH)_3(COOH)_1$ (labeled as GOM1), $C_{54}H_{15}(O)_2(OH)_5(COOH)_1$ (represented by GOM2), and $C_{54}H_{12}(O)_3(OH)_7(COOH)_1$ (denoted by GOM3). The GOM1 model has three OH groups, one epoxy, and one carboxylic acid group. The GOM2 structure has five OH, two epoxy, and one COOH group. There are seven OH, three epoxy, and one COOH group in the

GOM3 structure. The model structures were subjected to ground state optimization at Becke's three-parameter functional and Lee-Yang-Parr hybrid functional (B3LYP) computation level on the Gaussian 16 program [Frisch et al. (2016)]. The 6-31++g (d,p) basis set was used for the C, H, and O atoms in these calculations.

TD-DFT calculations were carried out to calculate the excited state properties of the model [Nakata et al. (2006)]. The optimized (ground state) GOM1 model was used as the input model for finding the singlet excited states by the TD-DFT calculations. The TD-SCF method/B3LYP functional/6-31++g (d,p) basis sets were employed for these calculations to find the excited state HOMO and LUMO locations. All calculations were in the gaseous phase.

5.3.2 Classical Molecular Dynamics Simulations

MD simulations were conducted only with the GOM1 model system (from the DFT calculations). The OG molecule (molecular formula: $C_{16}H_{12}N_2O_7S_2$) was constructed using GaussView 6 and optimized by the B3LYP hybrid functional using the 6-31++g (d,p) basis set. All model systems for MD simulations were constructed with the MAPS 4.1.1 software. The first step for the preparation of the initial model MD simulations was placing two GO1 entities in the central portion of a (75Å× 75Å × 75Å) cubical simulation box. The next stage was inserting 2000 H_2O, 4 OG, and 100 H_2O_2 molecules randomly in the rest of the cubical simulation box. The water molecules were modeled by the simple point charge (SPC) model [Mark & Nilsson (2001)]. Table 5.1 mentioned the charges on water model were used in this simulation. The Drieding force field parameters (12-6 Lennard-Jones) were implemented for GOM1, OG, and H_2O_2 molecules and their inter-atomic interactions [Mayo et al. (2002)]. Periodic boundary conditions were applied in all three dimensions. The Nose-Hoover thermostat controlled

the system's temperature at 298K with a damping factor of 10 ps. The non-bonded Van der Waals interactions were executed with a cut-off of 12 Å.

Table 5.1 Charges on water model used in the simulations.

Atom type	Charge
OW	-0.820
HW	0.410

The initial model was optimized by the sequential application of the steepest descent and conjugate gradient methods. Next, the system was subjected to an NPT ensemble simulation for 500ps to reach 1g/cc density. Finally, an NVT ensemble simulation was run for 20 nanoseconds with a time step of 1 femtosecond to understand different reactants' adsorption behavior on the graphene oxide sheets. All simulations were run using the LAMMPS program.

5.4 Results and Discussion

5.4.1 Characterization

Figure 5.1 shows the XRD spectra of G1 and G2 samples. The XRD pattern of G1 displays a sharp peak at 2θ = 10.24°, corresponding to the (001) plane and the interlayer spacing (d) of 0.86nm [Krishnamoorthy et al. (2013)]. There are two peaks in the XRD of the G2 sample. These are at 2θ =11.06° (d spacing is 0.79 nm), and a smaller (and broader) peak at 2θ = 23.20°. The peaks of G2 are at higher 2θ values corresponding to lower d values (shown by a purple dashed line in Figure 5.1) than those observed in G1. This shift points to fewer interlayer oxygen functional groups in G2 or a relatively more reduced GO species.

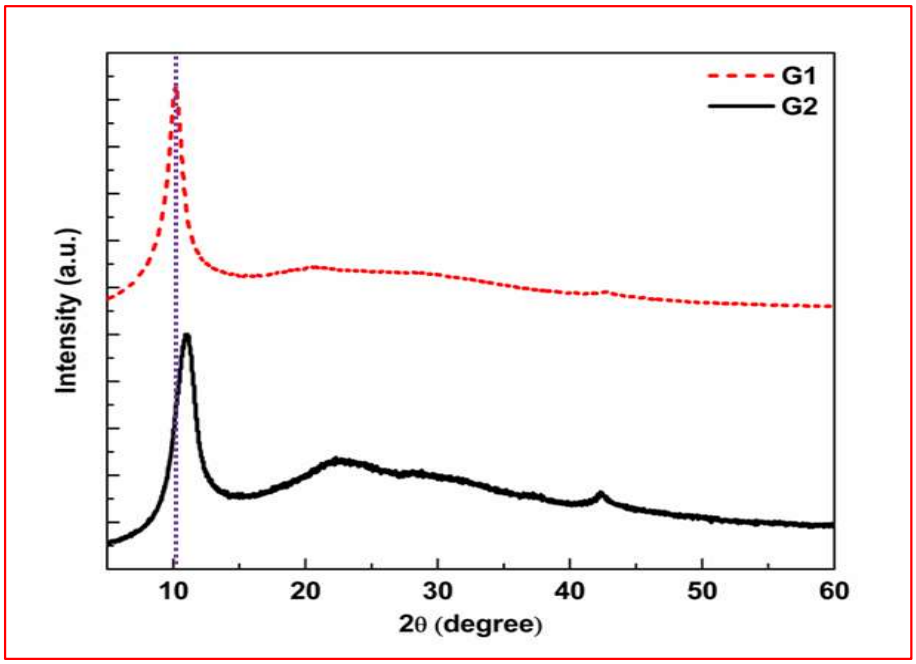

Figure 5.1 The XRD patterns of G1 and G2 powder samples.

Figure 5.2 represents the FT-IR spectra of G1 and G2 of powdered samples. The peaks at 3402cm^{-1} and 1380cm^{-1} are due to the stretching and (-C-O-H) bending vibrations of hydroxyl groups. These are present in both G1 and G2 samples. The peak at 1714cm^{-1} is the carbonyl group (C=O), stretching vibration, while the absorbance at 1623cm^{-1} confirms the presence of C-C stretching [Krishnamoorthy et al. (2013)]. The peaks at 1220cm^{-1} and 1056cm^{-1} are a consequence of the epoxy and alkoxy bending vibrations, respectively [Lee et al. (2016)]. Overall this shows the presence of the carboxylic functional group on both GO samples. Sample G2 FTIR also displays an absorbance at 2930cm^{-1} because of a CH_2 stretching vibration. This particular peak is also present in the G1 sample but has lesser intensity.

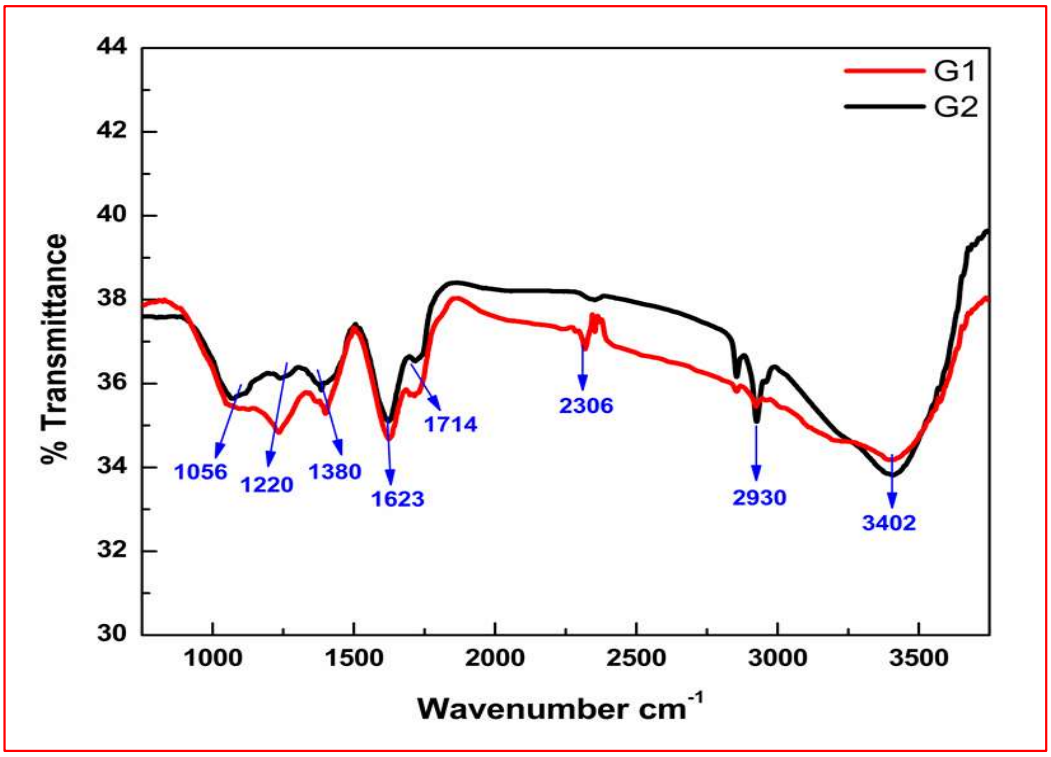

Figure 5.2 The FTIR spectra of G1 and G2 powder samples.

Figures 5.3a and 5.3b show the SEM images of G1 and G2 surface morphologies. The images show that the prepared GO sheets have uniform surfaces with small wrinkles on them. A larger number of layers seem to be agglomerated in the G2 sample.

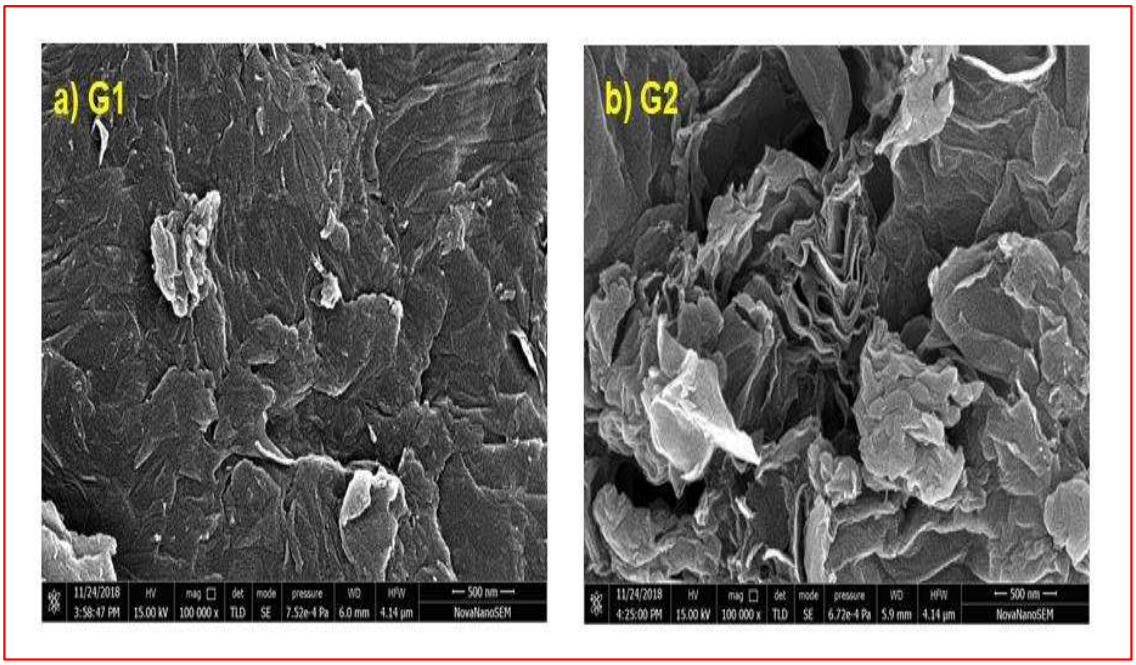

Figure 5.3 SEM images of G1 and G2 samples.

Figure 5.4a shows the UV-vis spectra of G1 and G2 samples. Both G1 and G2 show UV-visible signatures at 230nm due to π-π^* transitions. G2 also exhibits a small shoulder peak at 300nm due to n-π^* transitions. The color of the GO sample changes with its oxidation levels [Krishnamoorthy et al. (2013)]. The UV-visible data fits a direct band gap Tauc plot relation. Figure 5.4b displays these Tauc plots for G1 and G2 samples. The plots were drawn between $(\alpha h\nu)^2$ versus energy ($h\nu$ in eV) for finding direct transition bandgaps. The intercept of linear fits to these plots extrapolated to the x-axis gave the bandgaps. Samples G1 and G2 have direct bandgaps of 2.5 eV and 2.0 eV, respectively The bandgap got reduced because of lesser oxidation in G2, which is corroborated by the smaller d-spacing (XRD analysis) in it.

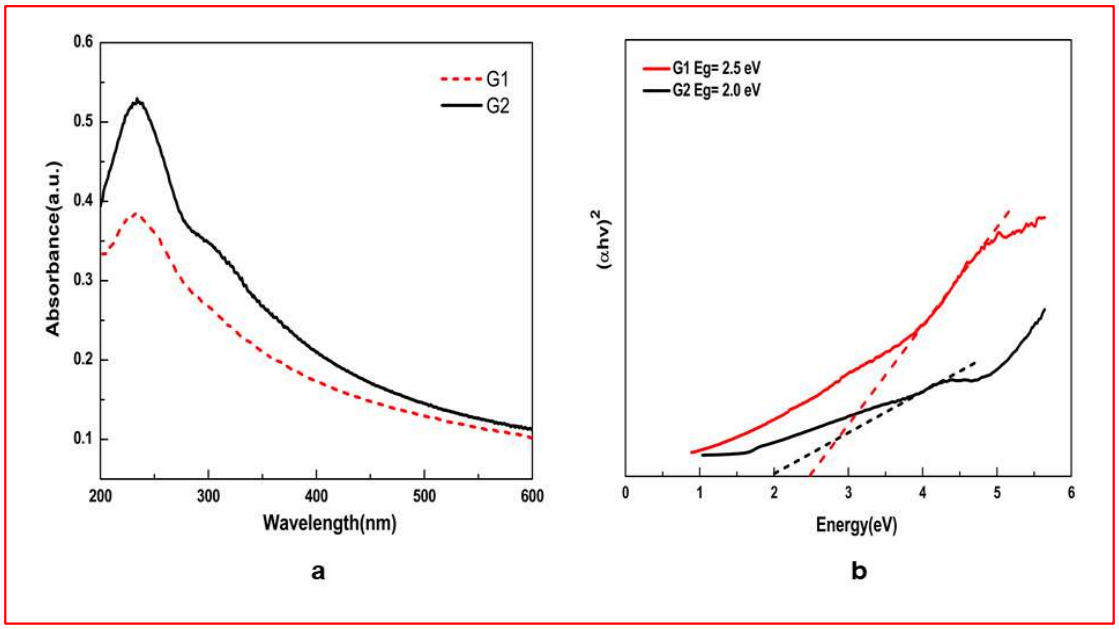

Figure 5.4 a) UV-Vis absorption spectra of G1 and G2 samples and b) Tauc plots for direct band gap calculation of G1 and G2 samples.

5.4.2 Photo-Fenton experiment analysis

The OG aqueous solution UV-spectrum displays three characteristic absorption peaks at 235, 331, and 475 nm due to benzene rings, naphthalene rings, and azo bonds (N=N), respectively (shown in Figure 5.5).

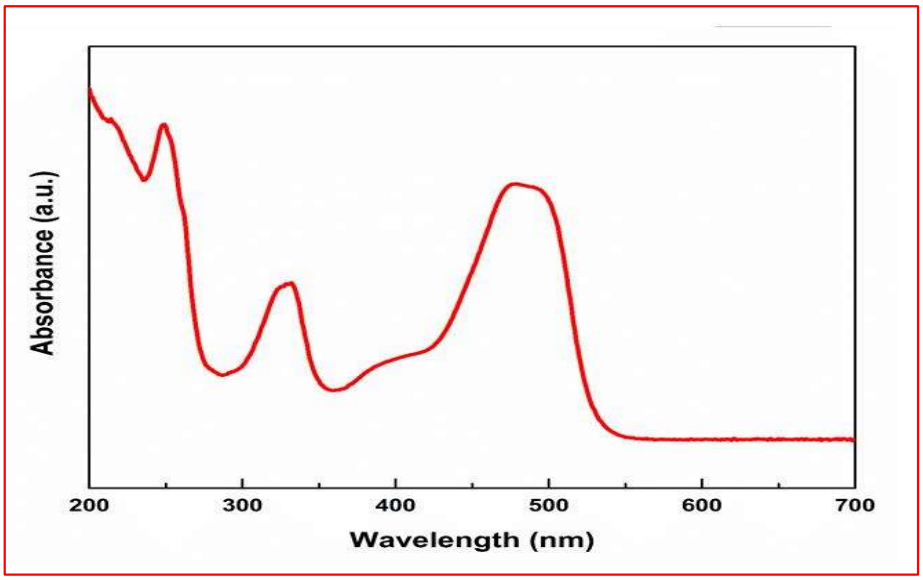

Figure 5.5 UV Visible spectra of Orange-G dye.

Figure 5.6 shows the effect of visible light irradiation on the UV–visible spectrum of a mixture of H_2O_2 and OG (in the absence of any catalyst) with time. Very little change occurred in this spectrum with time. Thus, H_2O_2 does not affect OG dye in the acidic medium under visible-light irradiation (in the absence of any catalyst).

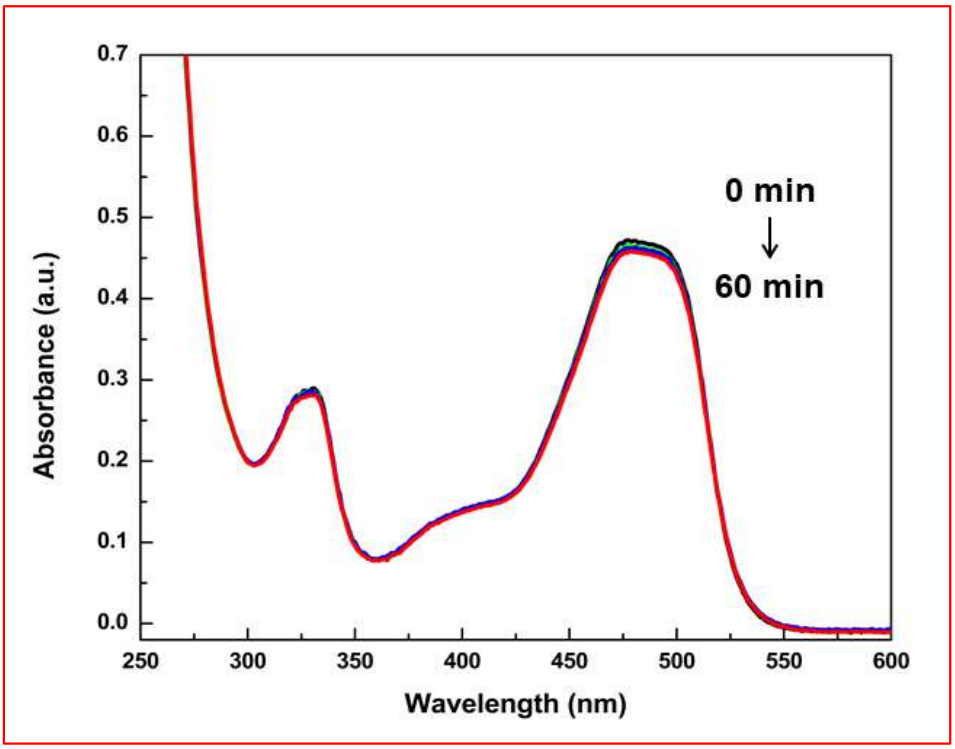

Figure 5.6. UV-visible plots of degradation of Orange-G dye at regular intervals of reaction time in the presence of only H_2O_2 under light conditions (without catalyst).

Next, the heterogeneous Fenton-like degradation of OG dye was checked in the dark after adding the same amount of G1 or G2 materials. There was no OG degradation with the G1 catalyst in the dark. Nevertheless, about 10% OG got degraded (Figure 5.7) when the Fenton-like reaction was carried out on the G2 catalyst for the same interval of time (~100 minutes).

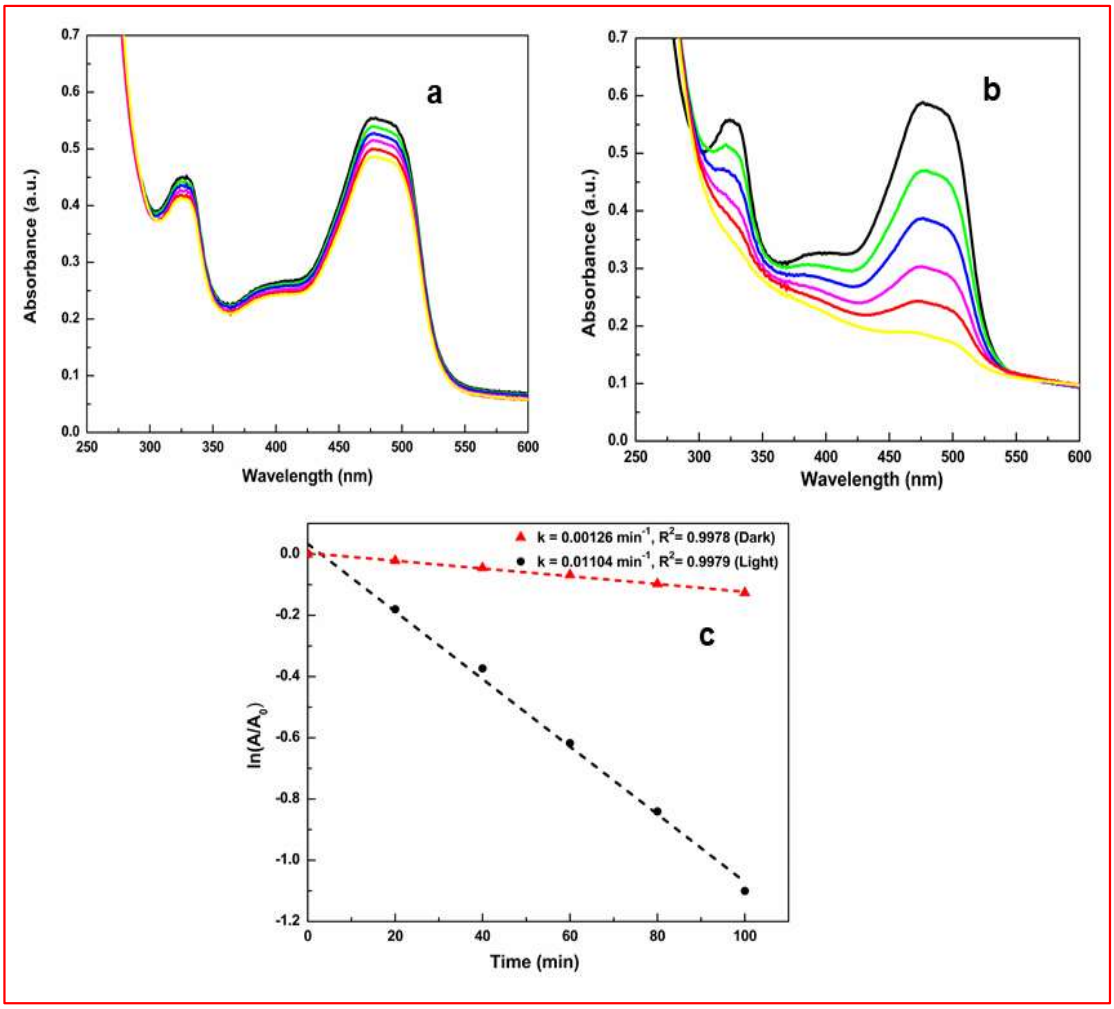

Figure 5.7 UV–visible absorbance plots of Fenton degradation of OG with time (100 minutes reaction time) catalyzed by G2 catalyst a) dark and b) light conditions, respectively. c) Comparision of rate kinetics of OG degradation on G2 sample under different conditions.

On irradiation by cool white LED visible light (photo-Fenton-like conditions), OG got almost fully degraded in 140 minutes on G1 and 100 minutes over G2 photocatalyst, respectively (Figure 5.8a and 5.8b). The photo-Fenton OG degradation (Figure 5.8c) followed first-order kinetics over both G1 and G2. The visible light photocatalysis over the G2 catalyst was substantially faster than on G1. Moreover, the kinetics of G2 catalyst

under visible light is ten times than in the absence of light. These results suggest that visible light enhances the photo-Fenton activity of G2 appreciably.

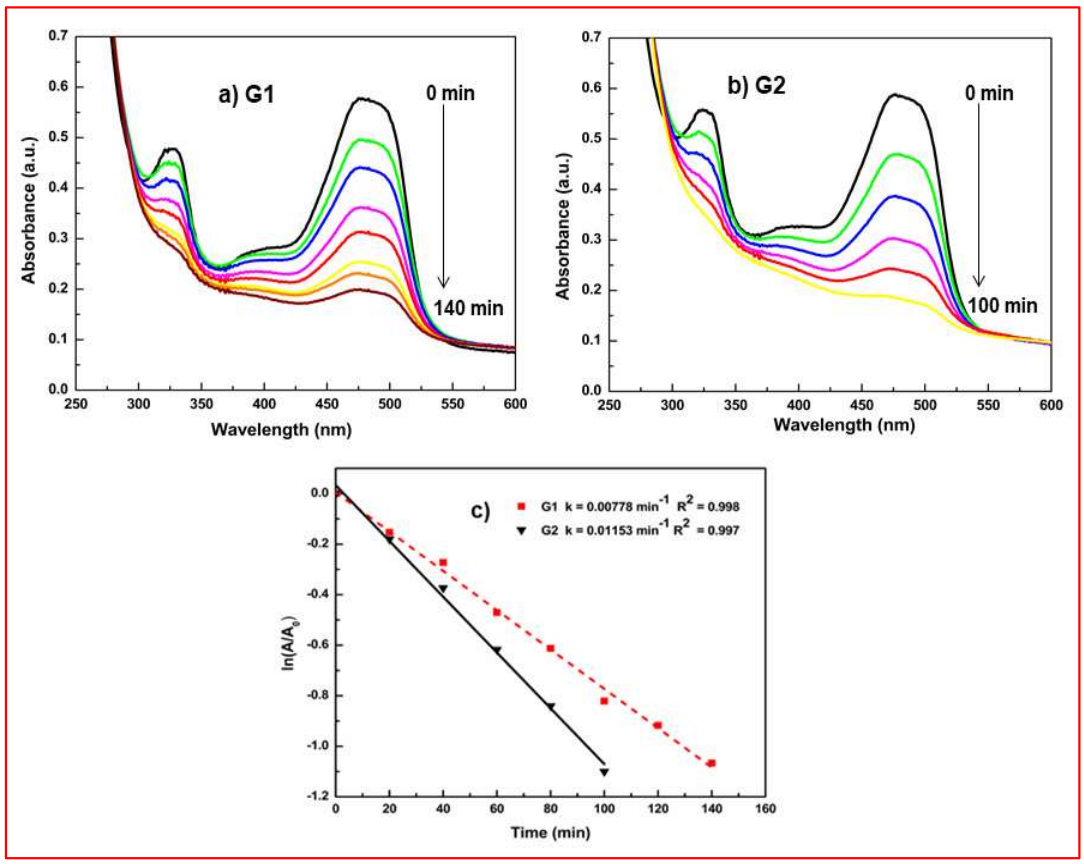

Figure 5.8 UV–visible absorbance plots of photo-Fenton degradation of OG at regular intervals of reaction time (under light conditions) catalyzed over a) G1 and b) G2 photocatalyst. c) The plots of $\ln(A/A_0)$ [absorbance (A) measured at $\lambda_{max} \sim 475$ nm] versus time for (OG degradation) reactions catalyzed by G1 and G2 catalysts.

5.4.3 Recyclability test

The reusability of G1 and G2 photocatalysts for OG degradation were also evaluated (Figure 5.9). The photocatalysts were recycled three times each. Both photocatalysts showed good activity until the third cycle. While G1 demonstrated almost ~90% (of the first cycle) photocatalytic activity at the end of its third reuse, for the same reuse, G2 activity decreased to ~80% of its first cycle.

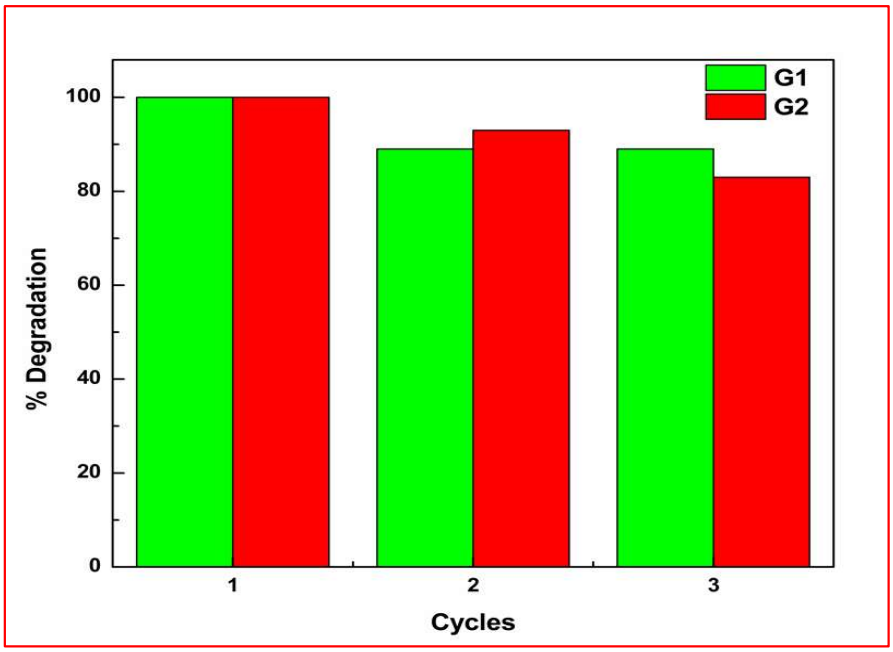

Figure 5.9 Recyclability of G1 and G2 catalysts for OG degradation in 100 minutes.

5.4.4 Computational analysis

Figure 5.10 displays the three geometry optimized GO model structures (GOM1, GOM2, and GOM3). It also gives the HOMO-LUMO gaps (E_g, energy gap) corresponding to these optimized structures. The calculated gaps are 1.73 eV, 2.04 eV, and 2.11 eV for GOM1, GOM2, and GOM3. The energy gap of a GO structure increased with the hydroxyl and epoxy group coverages. The pattern of changing band gap with oxygen functionalities is consistent with a study done by Huang et al. (2012). Next, DFT calculations were employed to find the nucleophilic (or HOMO location) centers in the ground state GOM1 optimized structure (corresponding GO in the dark) because it has the smallest HOMO-LUMO gap. Then TD-DFT calculations were carried out to ascertain the nucleophilic centers in the excited state GOM1 structure (corresponding to a photo-excited GO).

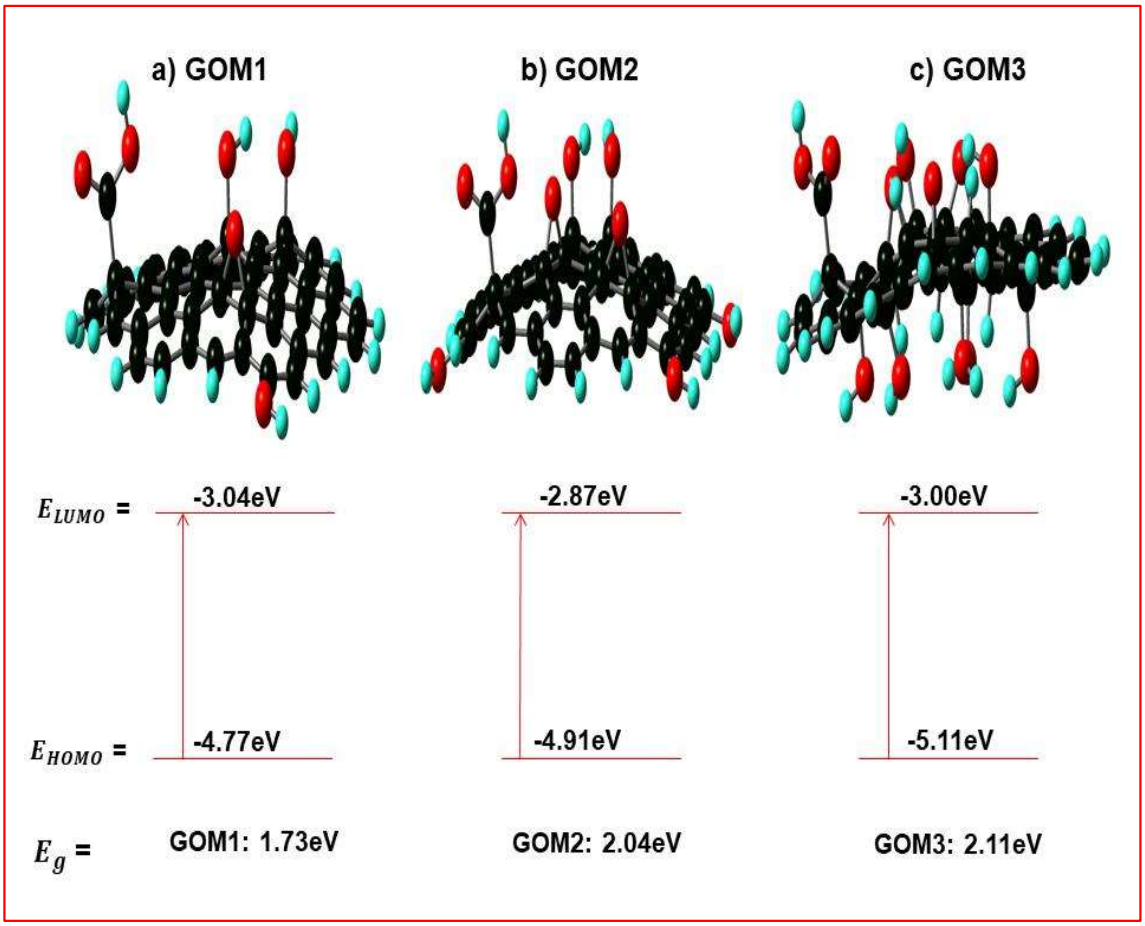

Figure 5.10 Optimized structures and HOMO-LUMO gaps of a) GOM1, b) GOM2, and c) GOM3.

Figures 5.11a and 5.11b display the locations of HOMO and LUMO in the ground state GOM1 structure. The HOMO in ground state GOM1 structure primarily resides on the carbonyl part of the COOH group and the carbon atom adjacent to it, while LUMO is on the OH and epoxy groups (Figure 5.11b). Furthermore, there are almost no LUMO on -COOH and carbon adjacent to it. Figure 5.11c and 5.11d show HOMO and LUMO positions in the TDDFT calculated excited state GOM1 structure. Figure 5.11c displays that HOMO is mainly on the epoxy group, and this is the typical nucleophilic center in a photo-excited GO structure. The position of the nucleophilic portion is (mainly epoxy group) is shown by the red circle.

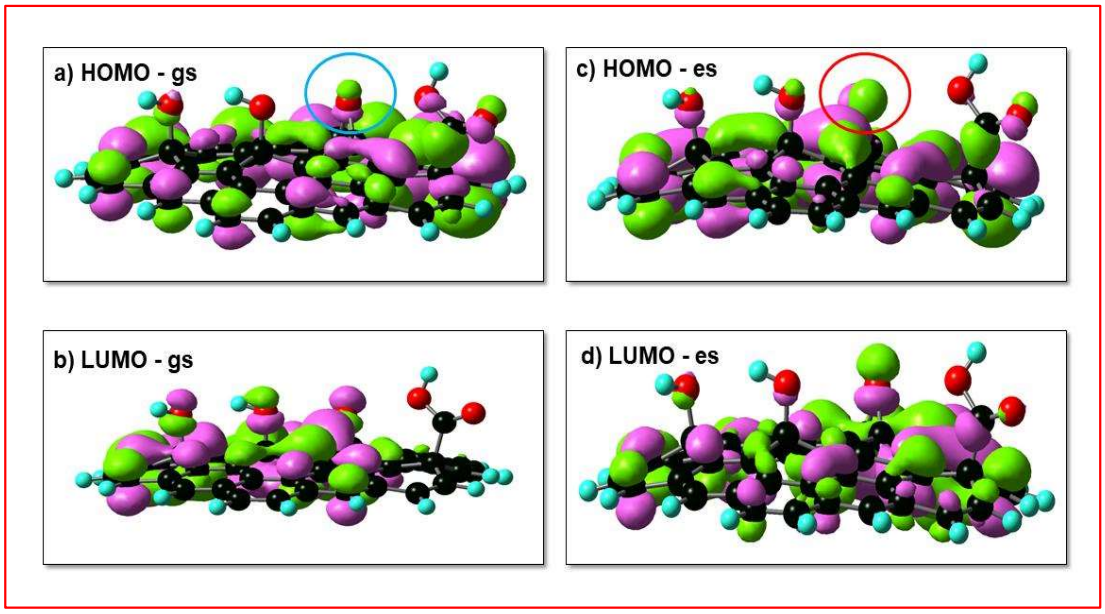

Figure 5.11 a) HOMO (ground state) and b) LUMO (ground state) by DFT calculation, c) HOMO (excited state) and d) LUMO (excited state) by TDDFT calculation.

Figure 5.12a is a representative snapshot of the MD simulation output after a long equilibration run. The green and blue colored molecules depict H_2O_2 and OG molecules, respectively, while the yellow-colored entity represents the GOM1 monolayer sheet. Nevertheless, such a snapshot does not give the average or representative scenario over a long-time interval. Long-time average radial distribution functions (RDF) between various atom types in two different entities (like GOM1 and H_2O_2) can give the relative strength of interaction.

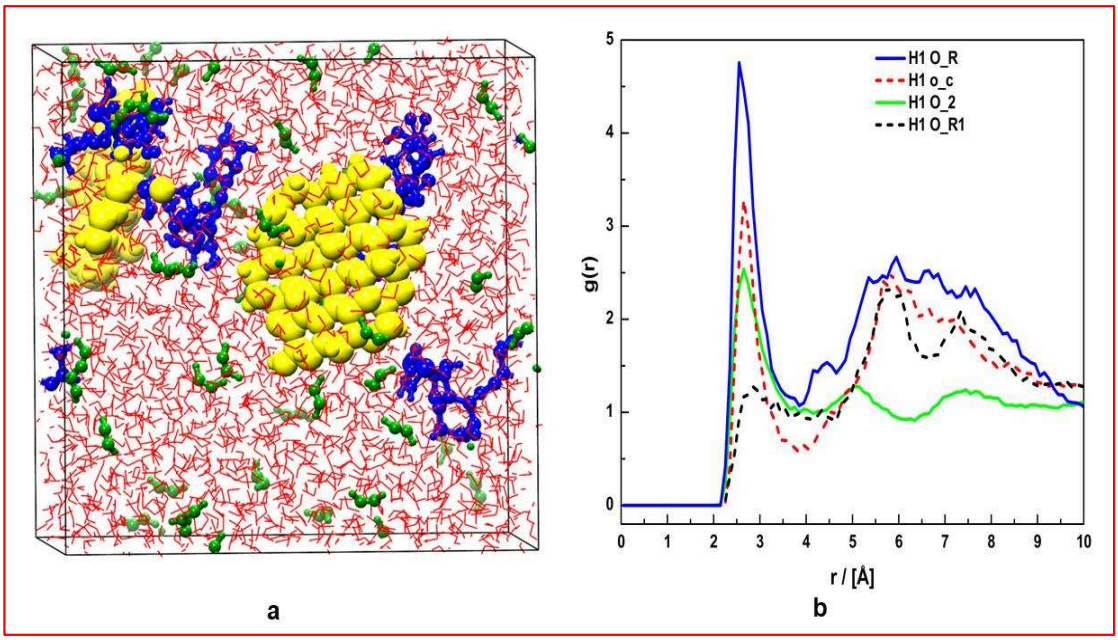

Figure 5.12. a) Snapshot obtained after long equilibration run. and b) RDF curve of different interactions of H_2O_2 with Graphene oxide (GOM1). [Convention followed in the RDF- H1: Hydrogen atom in H_2O_2, O_31: oxygen atom in H_2O_2, O_R: epoxy oxygen atom present in GOM1, o_c: Keto group oxygen atom of COOH present in GOM1, O_2: oxygen atom of Hydroxy functional group present in GOM1, O_R1: Hydroxy group oxygen atoms attached to a carbon atom in COOH group is present in GOM1.

Figure 5.12b shows such RDFs between atom types making various functional groups in GOM1 and H_2O_2. The first peak (2.5 Å) in an RDF is the smallest distance at which the two atom types (being considered) have a high interaction probability. As mentioned earlier, there are three types of functional groups (hydroxyl, epoxy, carboxy) in the GOM1 model. The most intense blue peak (H1-O_R) represents the interaction between the hydrogen of H_2O_2 molecules and the epoxy group's oxygen atom present on GOM1. The RDF peak representing the interaction between the hydrogen of H_2O_2 molecules and the carbonyl oxygen (on GOM1) occurs at the same distance (dashed red curve, H1-o_c), but its intensity is about 30-35% lower than the H1-O_R peak. The H1-O_2 (the solid green plot) peak also coincides with the ones mentioned above, but its intensity is only 50% of the dashed black plot.

The interaction of (H_2O_2) oxygen with the GO functional groups is displayed in Figure 5.13. The blue plot (O_31-HB) with its first (broad) peak at ~2.6 Å gives the interaction between the oxygen of H_2O_2 (O_31) with the hydrogen (HB atom type) of the hydroxyl group in GO. This peak is complementary to the RDF of interaction between the hydrogen of H_2O_2 and oxygen of the hydroxyl functional groups on GO. Therefore, it appears at an approximately similar distance but with reduced intensity.

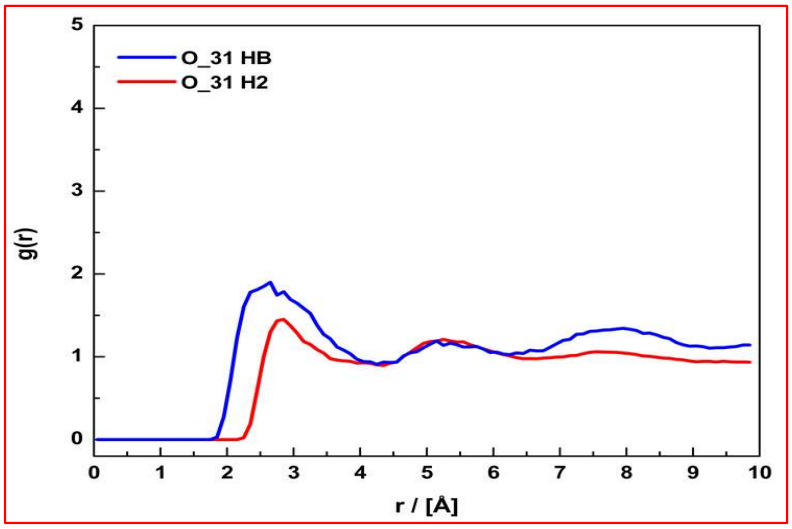

Figure 5.13. RDF curve of Oxygen atom type of H_2O_2 with functional groups of GOM1 model. [Convention followed in the RDF- O_31: oxygen atom in H_2O_2, HB: Hydrogen atom type in OH group present in GOM1 model and H2: Hydrogen atom in COOH group present in GOM1 model].

The O---H intermolecular distance $R_{OH} \leq 2.5$ Å is defined as a typical hydrogen bond distance. This distance was derived by authors of previous reports [Singh & Verma (2018), Silvestrelli & Parrinello (1999)] from the first minima of the RDF of H_2O molecules. Our RDF first peaks (Figure 5.12b) between the oxygen atom type of GO functional groups and the hydrogen of H_2O_2 also lie at 2.5 Å. Hence, it can say that H_2O_2 molecules primarily adsorb on the GO surface through a hydrogen bond type interaction.

In contrast to the above, the RDF of H_2O_2 with atom types in OG displays the first peak only at a distance of 3.5 Å (Figure 5.14). Furthermore, the intensity of the dashed red plot giving interaction of oxygen atom in H_2O_2 with the carbon atoms in benzene and naphthalene rings of OG molecule is substantially lesser than the H1-o= (the dashed green plot) peak. Hence, the interaction between OG and H_2O_2 molecules is weak. This MD result is substantiated by the experimental observation that there is no OG degradation when it is added to an H_2O_2 aqueous solution in the absence of any catalyst.

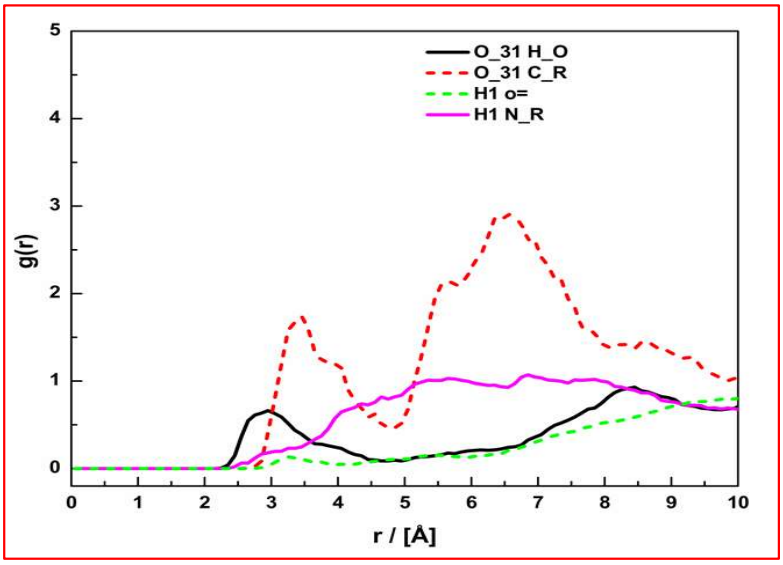

Figure 5.14. RDF curve of different interactions of H_2O_2 and Orange-G(OG). [Convention followed in the RDF- H1: Hydrogen atom in H_2O_2, O_31: oxygen atom in H_2O_2, H_O: hydrogen atom of hydroxyl group present in OG, C_R: carbon atoms present in rings of OG molecule, o=: oxygen atom are atoms to sulfur in OG molecule, N_R: nitrogen atom present in the OG molecule azo bond]

5.4.5 Mechanism

This section combines the computational and experimental results to deduce the possible heterogeneous photos-Fenton mechanism of OG degradation on GO (Figure 5.15). The

ground state DFT calculations show that the HOMO is located on the carbonyl part of -COOH functionalities on the GO surface. MD results show that H_2O_2 interacts strongly with epoxide functionality but its adsorption to GO through the carbonyl part is much weaker. Note that H_2O_2 undergoes reductive cleavage for $^{\bullet}OH$ generation. Consequently, H_2O_2 needs to interact with nucleophilic catalytic sites for its efficient reductive cleavage. Since the carbonyl part of -COOH functionalities are the nucleophilic sites on GO sheets; therefore, H_2O_2 attachment to GO mainly through the epoxide functionality results in poor $^{\bullet}OH$ generation. The inferior Fenton-like GO activity in the dark for OG degradation (Figure 5.7a) is in agreement with this computational inference.

Photo-Fenton-like organic pollutant degradation using H_2O_2 requires efficient $^{\bullet}OH$ generation [Ojha et al. (2017)] on the photo-excited GO surface. TD-DFT calculations simulated the excited states of the GO structure, analogous to its photo-excitation. These calculations show that the HOMO shifts to the epoxide functionality on the GO surface in the excited state. Hence, in the excited state, the epoxide functionalities become the nucleophilic sites on the GO surface. As mentioned earlier, the MD results tell us that H_2O_2 adsorbs strongly with GO through its epoxide functionality. The strong interaction of H_2O_2 molecules with GO through its (excited state) nucleophilic (epoxide) sites lead to substantially more effective reductive cleavage of the former and thereby $^{\bullet}OH$ generation. The considerably faster OG degradation (Figure 5.7c) on visible light irradiation of GO (than in the dark) validates the preceding inference.

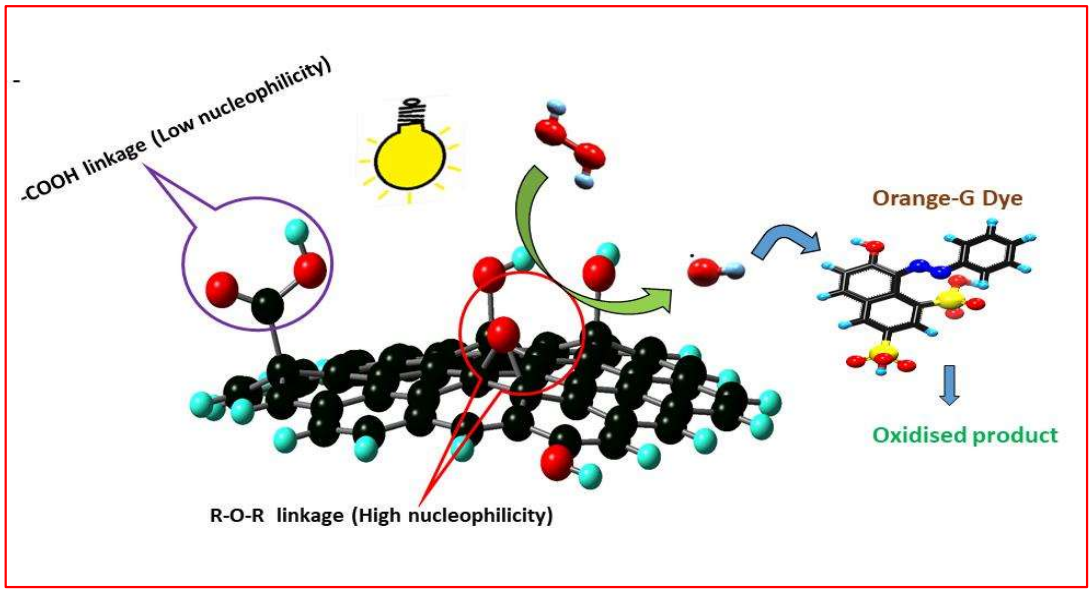

Figure 5.15 Photo-Fenton degradation mechanism of orange G dye on the GO surface.

5.5 Conclusions

The Fenton (in the dark) and visible light photo-Fenton catalytic mechanisms of two GO materials (GO1 and GO2) with different degrees of oxygen functionalities are investigated for orange-G (OG) dye degradation. Both GO materials have bandgaps in the visible range, and they demonstrate significantly better activity under visible light photo-Fenton conditions than for the Fenton (in the dark) reaction condition. Furthermore, the GO material with the smaller bandgap (GO2) exhibits better photo-Fenton activity for orange-G degradation. DFT and TD-DFT calculations results showed that photo-excitation shifts the HOMO from the carbonyl part to the epoxy functional group on the GO surface. Large-scale MD studies demonstrated the preference of H_2O_2 to adsorb to the epoxy part, while the orange G moiety is located nearby. Because of stronger H_2O_2-GO epoxy interactions, the reaction catalyzed under photo-Fenton conditions exhibits significantly higher orange G degradation activity than in the Fenton circumstances. The present investigation demonstrates that such a combination of DFT and MD studies can screen photocatalysts for a precise target reaction.